



# Laser welding of 16MnCr5 butt welds with gap: resulting weld quality and fatigue strength assessment

J. Hensel<sup>1</sup> · M. Köhler<sup>2</sup> · L. Uhlenberg<sup>2</sup> · J. Diniz e Castro<sup>2</sup> · K. Dilger<sup>2</sup> · M. Faß<sup>3</sup> · J. Baumgartner<sup>3,4</sup>

Received: 20 October 2021 / Accepted: 21 April 2022 / Published online: 29 April 2022  
© The Author(s) 2022

## Abstract

For laser welding, gaps should normally be avoided to ensure stable weld processes and high weld quality. Nonetheless, sometimes, gaps are resulting from non-optimal weld preparation in industrial applications. Within this investigation, the effects of a defocussed beam and laser beam oscillation on gap bridging abilities at reduced ambient pressure were investigated. For reference purpose, conventional laser welding with zero gap at ambient pressure was performed, too. The resulting weld geometry was investigated and correlated to gap bridging strategies and weld quality groups according to ISO 13919–1. The welds were characterized regarding their hardness and weld microstructure. Residual stress was determined by means of X-ray diffraction, and tensile tests as well as fatigue tests were conducted. The fatigue tests were evaluated by the nominal stress approach, the critical distance approach, and the stress averaging approach and correlated to weld quality measures. Resulting from this, fatigue resistance of laser welded butt welds with gap can be estimated by the FAT160 design S–N curve. The stress evaluation parameters for the determination of  $k_{eff}$ -values ( $\rho^* = 0.4$  mm,  $a = 0.1$  mm) were confirmed.

**Keywords** Laser beam welding · 16MnCr5 · Fatigue · Weld quality · Effective stress approach

## Abbreviations

A <sub>5</sub>	Elongation at fracture	ISO	International Organization for Standardization
BM	Base material	M	Weld profile evaluation path
CEV	Carbon equivalent	N	Number of load cycles
E	Young's modulus	R	Stress ratio
FAT	Fatigue resistance curve, as defined by IIW	R <sub>m</sub>	Ultimate tensile strength
FE	Finite element	R <sub>p0.2</sub>	Yield limit
HAZ	Heat affected zone	TIG	Tungsten inert gas
IIW	International Institute of Welding	T <sub>s</sub>	Scatter of S–N data
		TU	University of Technology
		WM	Weld metal
		a	Critical distance used in the critical distance approach
		cw	Continuous wave
		f(R)	Bonus factor applied for mean stress correction
		h <sub>1</sub>	Undercut depth
		h <sub>2</sub>	Excess penetration
		k	Wöhler curve exponent
		k <sub>eff</sub>	Effective stress
		m	Misalignment
		r <sub>ref</sub>	Reference radius used in the notch stress approach
		s <sub>g</sub>	Material parameter for the stress gradient approach
		t	Sheet thickness
		w <sub>1</sub>	Upper weld bead width
		w <sub>2</sub>	Weld root width
		Δ <sub>σ</sub>	Nominal cyclic stress range

Recommended for publication by Commission XIII - Fatigue of Welded Components and Structures.

✉ J. Hensel  
jonas.hensel@mb.tu-chemnitz.de

<sup>1</sup> Institute of Joining and Assembly, Chemnitz University of Technology, Reichenhainer Str. 70, 09126 Chemnitz, Germany

<sup>2</sup> Institute of Joining and Welding, Technische Universität Braunschweig, Langer Kamp 8, 38106 Braunschweig, Germany

<sup>3</sup> Mechanical Engineering Department, Research Group SAM, Technical University of Darmstadt, Otto-Bernd-Straße 2, 64287 Darmstadt, Germany

<sup>4</sup> Fraunhofer LBF Institute for Structural Durability and System Reliability, Bartningstr. 47, 64289 Darmstadt, Germany

$\Delta\sigma_{\text{eff}}$	Effective cyclic stress range
$\nu$	Poisson ratio
$\rho^*$	Averaging length used in the stress averaging approach
$w$	Weld flank angle
$\sigma$	Stress
$\sigma_{\text{eff}}$	Effective stress
$\sigma_{\text{max}}$	Maximum notch stress
$\sigma_n$	Nominal stress
$\chi^*$	Stress gradient

## 1 Introduction

Gaps present particular challenges for the proper formation of laser welded joints due to high beam quality and small focal diameters of modern laser beam sources. In consequence, the resulting weld geometry is unfavorable with regard to load bearing capacities, e.g., fatigue strength due to high local stress concentration. Advanced process strategies such as beam oscillation may be applied to intentionally broaden the weld width and overcome this problem [1–3].

Due to increasing efficiencies and the possibility of using flexible beam guidance systems, the use of solid-state laser sources is preferred for industrial welding tasks today. Compared to conventionally used CO<sub>2</sub>-laser sources, the use of solid-state lasers results in increased weld spatter formation during welding. However, this can be countered by using a reduced ambient pressure in the process environment. In addition, recent developments towards precise welding with higher beam qualities and smaller focus diameters place high demands on the manufacturing accuracy of the components to be joined. Laser beam welding is usually conducted at zero gap. However, due to manufacturing tolerances, gaps cannot always be avoided. Next to the resulting process instabilities, the weld geometry is affected negatively from gaps. High local stress concentration results as consequence from sharp geometric notches, which affects service properties such as ultimate strength and fatigue life. Effects of weld quality on fatigue life were studied before and the significance of high-quality welds for safe operational use of structural components is evident [4].

This article presents research on laser welding of 16MnCr5 butt welds with and without gap. Specimens welded at ambient pressure without gap are presented as reference. Specimens with gap were welded at reduced ambient pressure for a reduction of weld spatter applying different gap bridging strategies, focussed, defocussed, and oscillated beam.

## 2 State of the art

### 2.1 Reduced ambient pressure and gap bridging in laser beam welding applications

A reduced ambient pressure in the welding environment has two major effects on the welding process during laser keyhole welding: A change in weld seam formation and reduced weld spatter formation [5–7]. Concerning the weld seam formation, several researches have shown that a reduced ambient pressure in the welding environment leads to narrower weld seams with a higher welding depth compared to welding at atmospheric pressure [8–11]. This is explained by the change in vapor pressure temperature of the material depending on the ambient pressure. At lower ambient pressure the material reaches the gaseous phase at lower temperatures whereas the melting temperature remains unaffected by the pressure change. Consequently, a lower energy input is sufficient to vaporize the material and initiate keyhole welding with increased welding depth. At the same time, the overall temperature in the molten pool decreases, causing the formation of a narrower weld seam cross-section and heat affected zone (HAZ). Additionally, the ambient pressure affects the flow conditions as well as the formation of the metal vapor plume. For laser beam welding at atmospheric pressure, a strong fluctuation of the metal vapor plume is observed, causing increased weld spatter formation by impulses on the keyhole rear wall and melt pool [12–14]. Furthermore, instabilities of the keyhole can cause the formation of weld spatter [15]. By suppressing the metal vapor plume and changing its flow conditions as well as the resulting stabilization of the keyhole, the risk of weld spatter formation decreases for the welding process at reduced ambient pressure. It was found, that an ambient pressure of < 10 hPa to a large extent leads to a suppressing of the characteristic vapor plume during solid state laser welding.

Welding at reduced ambient pressure shows great benefits in terms of efficiency and weld quality. However, due to the narrower weld seam formation gaps in the edge preparation pose a significant challenge. In general, joint preparation with gaps cause an unevenly absorption of the laser beam, resulting in an unsteady welding process. Due to instabilities in the keyhole and missing material for the joint formation, weld seam defects such as lack of fusion and undercuts may occur. Studies on the process reliability for laser welding of joints with gaps show significant dependencies on material, sheet thickness, weld joint geometry, and the process technology used. Described possibilities for increasing the gap bridging abilities primarily relate on the use of additional filler

material [16–18]. However, the use of filler wire in laser beam welding requires complex process control and an elaborate matching of the filler metal to the metallurgy of the base material. In order to avoid the use of additional filler material, another approach to improve the gap bridging properties is to increase the weld seam width [1]. This can be achieved by using a defocused laser beam or beam oscillation. Focusing on fillet and overlap welding of thin sheets, Albert et al. and Fixemer et al. used a linear oscillation in combination with a joint tracking device [19, 20]. By applying a beam oscillation perpendicular to the welding direction, gaps up to the sheet thickness for steel and 50% of the sheet thickness for aluminum could be successfully welded. Vänskä et al. reported on using beam oscillation to compensate for tolerances in weld preparation on stainless steel tubes by broadening the weld seam geometry [1]. Previous work by the authors conducted on butt joints also showed that a beam oscillation during laser beam welding at reduced ambient pressure leads to a broadening of the weld seam, thus resulting in enhanced gap bridging [21].

## 2.2 Influence of weld quality on fatigue

Weld fatigue is strongly dependent on stress risers such as axial and angular misalignment, the local weld geometry, e.g., weld flank angle, undercuts, and weld reinforcement and inner weld irregularities and flaws, such as pores and lack of fusion. These features and their magnitudes determine the weld quality and are summarized in technical standards [22, 23] regulating communication and requirements between structural designers and manufactures of welded components. The FAT classes of weld details according to IIW design recommendations for fatigue loaded structures [24] were related to weld fatigue earlier by Hobbacher and Kassner [25] for arc welds. They introduced the approach of weld imperfection tolerance and their classification with regard to weld detail and type of flaw. Lillemäe et al. investigated the effect of different arc welding technologies and their resulting weld geometries on fatigue of medium and high strength construction steels [26]. They proved a positive effect of base material strength for high quality welds in the finite life regime and at high numbers of load cycles. Hesse et al. investigated fatigue of beam welded steels and correlated weld geometry to resulting S–N curves, which demonstrated the potential of high quality beam welds [4]. They found similar beneficial effects for welds with low local stress concentration. Stenberg et al. reviewed possibilities of weld quality inspection in manufacturing of fatigue loaded welds and highlighted the importance of up-to-date standards for weld quality with regard to fatigue [27]. The importance of such an realistic quality consideration

was highlighted earlier by Kassner et al. under consideration of manufacturing conditions in the railway industry [28]. The misalignment and straightening during loading and its effects on resulting fatigue strength of thin sheets (3 mm and 4 mm) manufactured by various welding processes was investigated by Fricke et al. [29]. They proved an S–N curve slope exponent of  $k = 5$  being more suitable for sheets below 5 mm thickness. For thin laser welds, Liinalampi et al. demonstrated the effects of three-dimensional undercut geometry for fatigue strength [30]. They derived a correction factor under consideration of the ratio of weld width and undercut depth.

## 2.3 2.3. Fatigue strength assessment methods

Various approaches are available for the fatigue assessment of welded joints and structures [31]. They can be differentiated in approaches that consider the global stress distribution at the joint such as the nominal or structural stress approach or the local stress distribution directly at the weld such as the notch or effective stress approach. In the following, these approaches are shortly introduced and discussed in terms of their applicability for the assessment of laser-beam butt joints welded with and without gap.

### 2.3.1 Nominal stress approach

In the nominal stress approach, acting nominal stresses are compared to endurable nominal stresses that are collected for example in rules and guidelines such as [24]. Since global stresses are evaluated, the stress raising effects of a specific joint are not considered directly. Instead, the effect of the geometry on the fatigue strength is included in a separate FAT-class for each weld detail and failure mode, such as a transverse stiffener or a butt weld with weld toe, respectively, weld root failure.

If the weld geometry of the joint to be assessed differs significantly from the data that build the basis for the derivation of the FAT-class, this difference needs to be considered differently.

### 2.3.2 Notch stress approach with $r_{ref} = 0.05mm$

For the fatigue assessment of welded thin sheets, the notch stresses approach with a reference radius  $r_{ref} = 0.05mm$  is typically [32–34] used. Within this approach, the fatigue critical, sharp notches between two overlapping sheets, are rounded with this reference radius. The calculation of the maximum notch stresses is performed by a Finite-Element model and compared to endurable notch stresses that can be described by a class FAT630 [34]. From a methodical point of view, the notch stresses correlate to a stress intensity factor [32].

For the assessment of welded joints with failure from the weld toe, such as fillet welds, the reference radius approach needs to be modified [35, 36]. Due to larger notch opening angles at the weld toe radii, lower stress gradients and subsequently lower support effects are present. This leads to a reduction of FAT-classes and a dependency on the notch opening angle [37].

The application of the notch stress approach is limited to joints with a certain, minimum stress concentration. For welds with a notch opening angle  $\omega \leq 170^\circ$ , non-conservative results may occur [37]. This is also the case for welds with a non-defined toe radius such as for TIG-dressed [38] or mechanically ground joints.

### 2.3.3 Effective stress approaches

The effective stress approach based on the stress averaging approach according to Neuber builds the theoretical basis for the effective notch stress approach with a reference radius of  $r_{\text{ref}} = 1.0\text{mm}$  [39]. Whereas the application of the radius  $r_{\text{ref}} = 1.0\text{mm}$  is limited down to a sheet thickness of  $t \geq 5\text{mm}$  for weld toe failure and  $t \geq 10\text{mm}$  for weld root failure [37], the use of effective stresses in its original use can still be applied for thin sheets. In contrast to the notch stress approach with a reference radius of  $r_{\text{ref}} = 0.05\text{mm}$ , the effective stress approach can be used for welds with mild notches, large radii or distinct undercuts. For this, the real weld profile must be reflected in the FE-model.

Various different approaches exist to evaluate effective stresses and subsequently the influence of stress gradients on the fatigue strength:

- In the stress averaging approach [40, 41], the effective stresses are derived by an averaging of the stresses over a microstructural length of  $\rho^*$ .

$$\sigma_{\text{eff}} = \frac{1}{\rho^*} \int_0^{\rho^*} \sigma(x) dx$$

- In the critical distance approach [42–44], the effective stress is taken from a distance  $a$  in depth of the notch.

$$\sigma_{\text{eff}} = \sigma(x = a)$$

- In the stress gradient approach [45, 46], the stress gradients  $\chi^*$  are derived directly at the surface of the notch.

$$\sigma_{\text{eff}} = \frac{\sigma_{\text{max}}}{1 + \sqrt{s_g \chi^*}}$$

with

$$\chi^* = \frac{1}{\sigma_{\text{max}}} \cdot \frac{d\sigma}{dx}(x = 0)$$

All approaches contain a parameter [47] that describes the influence of the material on the support effects.

For the assessment of welded joints, the stress averaging approach as well as the critical distance approach lead to similar results [48]. With a critical distance of  $a = 0.1\text{mm}$  and a microstructural length of  $\rho^* = 0.4\text{mm}$ , the class FAT160 can be used for an assessment. It has to be mentioned that the parameters and the FAT class should depend on the material strength resp. hardness. However, a detailed identification has not yet been performed.

## 3 Applied methods and specimen characterization

The specimens used for this investigation were manufactured within two research projects at TU Darmstadt and TU Braunschweig. TU Darmstadt laser-welded reference specimens without gap at ambient pressure (plate thickness 4 mm) while TU Braunschweig focused on laser welding gap bridging strategies at reduced ambient pressure (plate thickness 2 mm). The here presented fatigue strength evaluation was conducted in close cooperation of the research institutes and is described in the following.

### 3.1 Experimental approach

The investigations were carried out using case-hardening steel 1.7131 (16MnCr5) in the unhardened condition. The nominal chemical composition is listed in Table 1. The combination of high hardness in the surface layer area (approx. 58–62 HRC) and favorable toughness makes case-hardening steels particularly suitable for the production of highly stressed transmission components, such as gears and shafts. Based on a low carbon equivalent (CEV = 0.54), case-hardening steels are generally considered conditionally weldable in the unhardened state.

Prior to sample manufacturing, basic investigations and process developments for welding at atmospheric (approx. 1000 mbar) and reduced ambient pressure (10 mbar) were carried out. For reference, specimens in zero-gap configuration were welded at atmospheric pressure. The zero-gap configuration was ensured by welding bead on plate. Furthermore, samples with gap were welded at reduced ambient pressure, using three process variations with different gap bridging abilities according to the parameters given in Table 2. The experimental setup for welding at reduced ambient pressure consists of a custom-made vacuum chamber with a volume of 0.25 m<sup>3</sup>. Within the chamber, an XY-cross table was used for weld specimen manipulation. The

**Table 1** Nominal chemical composition and mechanical parameters of 16MnCr5

Chemical composition in wt% (according to manufacturer specifications)						
Fe	C	Si	Mn	P	S	Cr
Bal	0.14–0.19	<0.40	1.00–1.30	<0.025	<0.035	0.80–1.10
Nominal mechanical parameters, condition of delivery (according to manufacturer specifications)						
Yield limit $R_{p0.2}$ in MPa				350 to 550		
Ultimate strength $R_m$ in MPa				530 to 680		
Elongation $A_5$ in %				10 to 25		

laser beam was guided into the vacuum chamber through two coupling glasses. The laser beam source used for the welding experiments was a TruDisk 6002 (Trumpf Laser- und Systemtechnik GmbH) diode-pumped Yb:YAG disk laser emitting at a wavelength of 1030 nm with a maximum output power of 6000 W and a beam quality of 8 mm\*mrad. The beam source was operated in continuous wave mode (cw). For the realization of a beam oscillation superimposed to the welding direction, a programmable focusing optic PFO 3D-2 (Trumpf Laser- und Systemtechnik GmbH) was used. The optical configuration in conjunction with an optical fiber (core diameter of 200  $\mu\text{m}$ ) for beam guidance resulted in a spot diameter of the laser beam at the focus position of 368  $\mu\text{m}$ . In addition to welding with a stationary laser beam, a geometrically freely programmable movement of the laser beam with a maximum deflection speed of 1000 mm/s can be realized.

To ensure constant gap properties along the weld seam and to minimize distortion related change in gap width, the samples with gaps were welded individually. Therefore, sheets with a width of 50 mm were welded in butt weld configuration. The additional width of the sample sheets in conjunction with the final sample geometry for mechanical testing further ensured, that weld start and stop positions were located outside the test cross section. The joint gap was set by inserting feeler gauge tape with a thickness of 0.2 mm at the end faces. The samples were then tack-welded at the end faces using tungsten inert gas welding. After tacking the specimens, the set gap dimension was checked and measured using a reflected-light microscope (Stemi2000, Zeiss). The investigations were based on an acceptance

range of a maximum deviation of 10% from the nominal gap dimension.

Laser-welded flat specimens made of 16MnCr5 were investigated under purely axial load. The external dimensions of the specimens welded without gap were 290 mm  $\times$  40 mm  $\times$  4 mm and with gap 170 mm  $\times$  40 mm  $\times$  2 mm, respectively. The geometry of the specimens is shown together with the testing machine at TU Darmstadt in Fig. 1. The tests of specimens welded without gap were performed on a resonance testing machine with a load ratio of  $R=0$  and a frequency of 57 Hz. Fatigue testing of samples with gap was performed at TU Braunschweig on a servo-hydraulic testing machine with a maximum dynamic load of  $\pm 80$  kN at a load ratio of  $R=0.1$  and a frequency of 20 Hz.

The micrographs and hardness of welds are shown in Fig. 2. Specimens welded with gap showed distinct undercuts (b and c) and significantly wider welds (c and d). The hardness of the base metal was in the range of 150 HV1 while the weld itself showed hardness of approximately 470...490 HV1, regardless the gap bridging strategy applied.

### 3.2 Weld geometry characterization

The surface profile measurements from the welded joints were carried out with the triangulation laser technique (type Micro-Epsilon optoNCDT1800). Since the welding process strategy for gap bridging had three different approaches within this study, the butt joints showed relevant geometrical variation at the weld notches among them (Fig. 3) and

**Table 2** Experimental parameters

Test series	Without gap	Gap, focussed	Gap, defocussed	Gap, beam oscillation
Joint type	Butt weld (full penetration welding)			
Plate thickness	4 mm	2 mm		
Welding speed	4 m/min	1.0 m/min		
Oscillation	-	-	-	Line
Focal position	-2 mm	0 mm	+8 mm	0 mm
Laser power	3500 W	850 W	1610 W	1400 W
Gap	0 $\mu\text{m}$	200 $\mu\text{m}$		

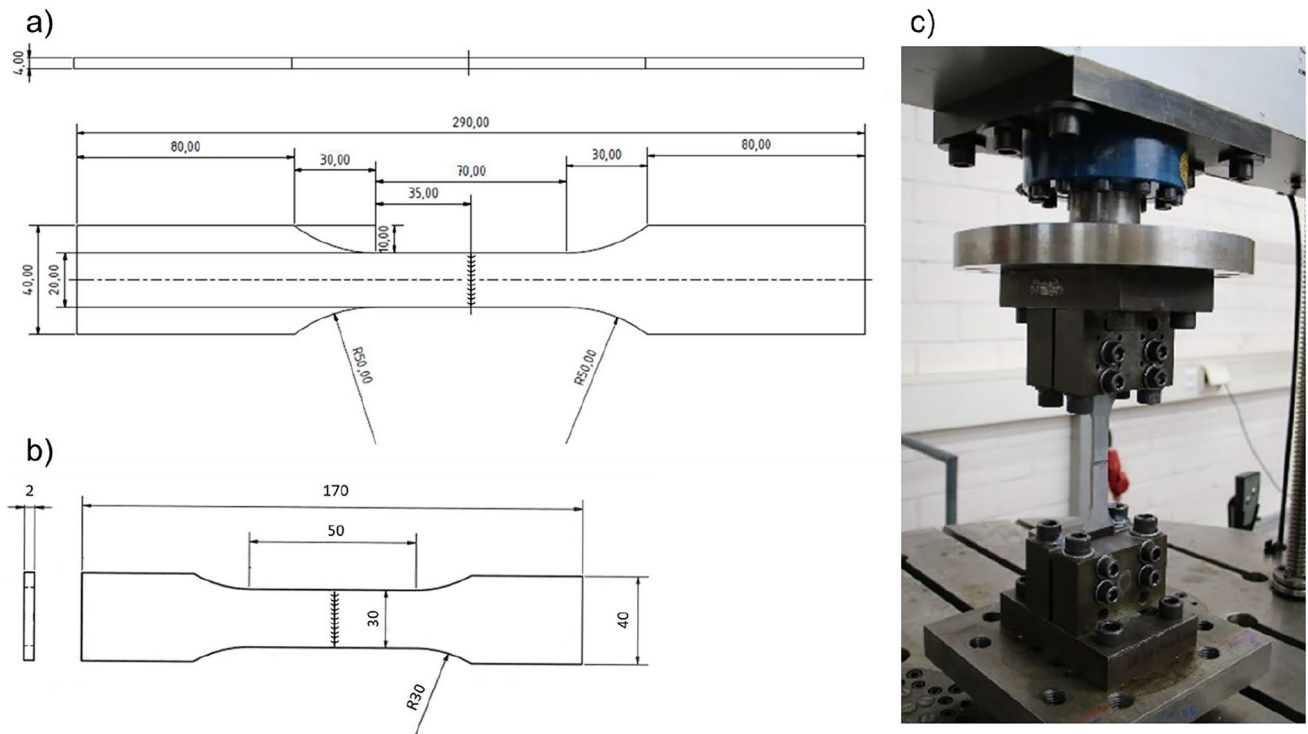


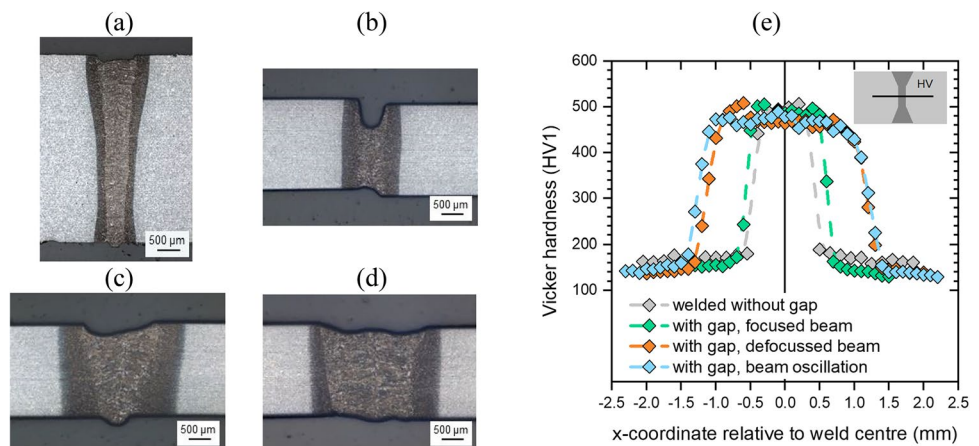
**Fig. 1** Specimen geometry for fatigue testing of laser welded flat specimens made of 16MnCr5 without gap (a) and with gap (b). c Fatigue testing machine in Darmstadt used for specimens without gap

consequently different quality aspects. Based on the macrographs and the graphics, it was possible to observe that the undercuts on the weld toe side  $h_1$  were larger than the excess penetration at the root side  $h_2$ , i.e., they can be more fatigue critical [30, 49]. It was also verified, that the misalignment  $m$  and excess penetration  $h_2$  were all included in the classification B from the specification standard ISO 13919–1 [23]. For the undercuts  $h_1$ , the quality ranged from C to D for the focussed beam and B to C for the defocussed and beam oscillation. All the parameters were in accordance with the maximum permitted values defined by the norm.

Specimens welded with gap and focussed beam showed relatively narrow welds with parallel fusion lines. The resulting weld undercuts  $h_1$  were relatively large compared to other test series. Wider welds resulted from defocussing and beam oscillation which helped to limit the occurring undercuts. Welding with defocussed beam created a V-shaped weld with distinct weld root, while the fusion lines of specimens welded with focussed and oscillated beam were more parallel.

To extend the seam geometry analysis, the ratio between the weld undercut depth and weld width ( $h_1/w_1$ ) was calculated. This value describes the shape and quality aspect of the

**Fig. 2** Weld seam cross-sections of specimens welded without gap (a) and different gap bridging properties using focussed laser beam (b), defocussed laser beam (c), and laser beam oscillation (d) and hardness (e)



quasi-elliptic notch [30]. The ratios for each process (welded without gap, welded with gap and focussed beam, defocussed beam and beam oscillation) are presented in Fig. 4. The range among them varied from 0.03 to 0.16 for specimens welded without gap respectively for specimens welded with gap from 0.16 to 0.64 for focussed beam, 0.07 to 0.19 for defocussed beam, and 0.02 to 0.12 for beam oscillation.

The ratio above mentioned was considered and evaluated in another studies, which confirmed its influence on the resulted stress notch for flat plates i.e., the deeper the notch is, compared to the length (sharper), the more the 2D and 3D analysis diverge [30, 49].

In the case of thin plates, there is no clear evidence of the correspondence between undercut depth and the fatigue strength [30]. Besides, the low fatigue strength and the scatter values can also be associated with higher undercut magnitudes and so higher ( $h_1/w_1$ ) ratio. This evidence can be observed in the S–N graphic presented in Fig. 11, where the results from specimens welded with gap and focussed beam correspond to a lower fatigue strength range and a more scatter values, confirmed by the higher ( $h_1/w_1$ ). The sum of these characteristics, e.g., higher depth undercuts, led to a narrower cross-section and consequently rose its nominal stress.

### 3.3 Residual stress

The residual stress was measured on the surface of fatigue test coupons by means of X-ray diffraction applying the  $\sin^2\Psi$ -method. The measurement was conducted on the side where fatigue cracks mainly initiated, e.g., the root side (specimens welded without gap) respectively the top side (specimens welded with gap). Residual stresses were determined along a line perpendicular to the weld in the specimen center, beginning from the weld into the adjacent base metal. Results for transverse and longitudinal residual stresses are presented in Fig. 5. The stress component transverse to the weld acted in fatigue loading direction.

In longitudinal direction all specimens showed tensile residual stress in the weld metal and the heat affected zone and compressive residual stress in the base metal. In fatigue loading direction (transverse to the weld) and at the location of fatigue crack generation, e.g., in the weld undercut, the focussed beam showed compressive residual stress of  $\approx -250$  MPa which was significantly higher compared to focussed beam and beam oscillation with  $\approx -80$  MPa.

### 3.4 Numerical modeling

#### 3.4.1 Model setup

The creation of the FE models was preceded by detailed measurements of the weld profile (compare the “Weld geometry characterization” section). These measurements were

obtained on multiple paths similar to M, see Fig. 6. The surface height progression (Y) over the length (X) of the specimens was measured along 10 differing lines spaced over the width of the specimen (Z). Out of these line-measurements, the presumed worst-case scan was used for modeling. The worst case for fatigue life was assumed to be depending on notch depth and sharpness.

The models were created as 2D models assuming a plane strain state in the z-direction, thus top and bottom surface contours along M are represented. Elements with quadratic shape function and a maximum element edge length of 0.02 mm on the surface were used. Material properties were set to the Young’s modulus  $E = 210$  GPa and the Poisson ratio  $\nu = 0.3$  assuming linear elastic material behavior. The boundary conditions approximated the real situation in the test rig: The specimens were modeled at full length between the clamping jaws of the test rigs (free length 130 mm). The specimens modeled contained misalignment as determined from laser profile scanning. At one end, all degrees of freedom were fixed. At the other end, the displacement in Y-direction was fixed and the one X-direction was allowed. The rotation was suppressed. A tensile force was applied in order to achieve a nominal stress of  $\sigma_n = 1$  MPa in the sheet. The influence of angular distortion and axial misalignment resulting from the welding process were considered by using the weld profiles as the basis for the models. In total 31 specimens were modeled this way: 13 welds with gap and focused beam, 10 with gap and defocused beam, 7 with gap and line oscillation, and 1 specimen welded without gap were simulated.

#### 3.4.2 Calculation results

Figure 7 shows the result image of a specimen welded with focused beam and gap for demonstration purpose. The picture visualizes the maximum principal stress field in the vicinity of the weld. A maximum stress of 10 MPa was reached right at the surface of the notch (marked by location B1). Due to the notch effect, the stress decreased quickly from there into depth direction (path from B1 to B2).

Results for further evaluation were obtained on path B1–B2 and on A1–A2. B1–B2 was selected as perpendicular to the surface from the maximum. The path A1–A2 follows the top surface of the specimen while being offset by 0.1 mm. For the stress averaging approach, the stress gradient along path B1–B2 was evaluated. Numerical extraction and evaluation of all values from the surface up to the microstructural length  $\rho^*$ , resp. critical distance  $a$  was performed. In order to visualize the effective stress by the critical distance approach along the surface, the stresses along a path A1–A2 in the depth of  $a = 0.1$  mm were additionally evaluated. In Fig. 8 some exemplary evaluations are shown for all specimen types. A large influence in terms of the evaluated maximum principal stress was identified between the four

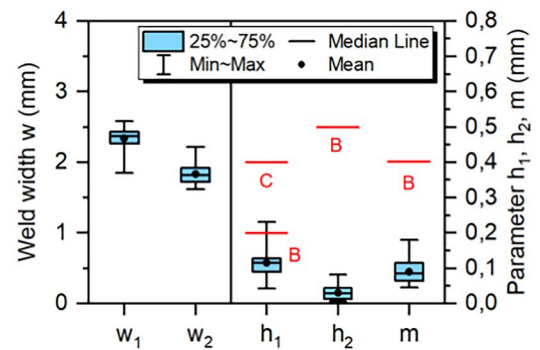
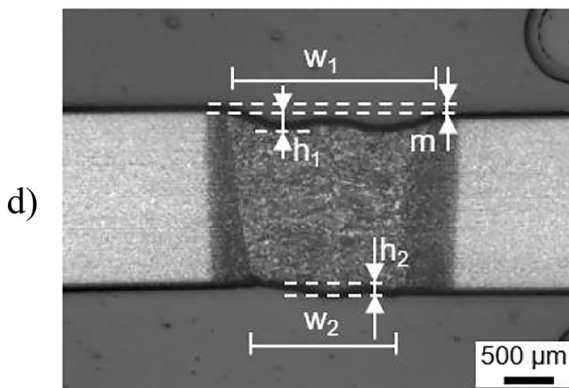
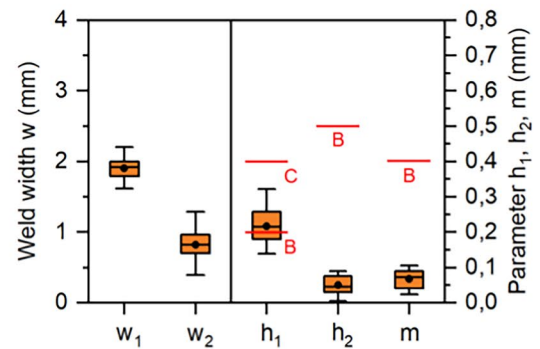
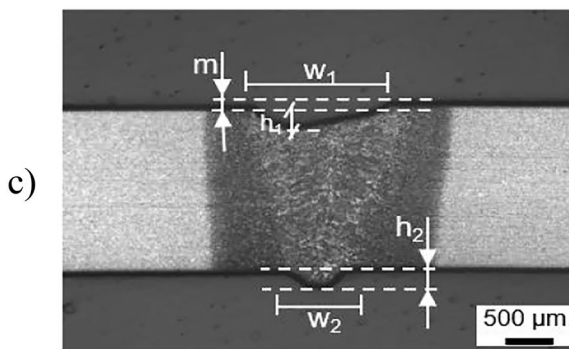
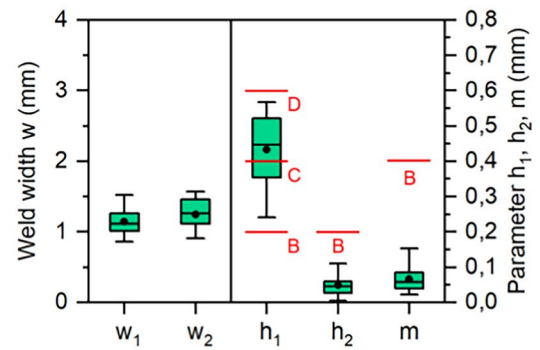
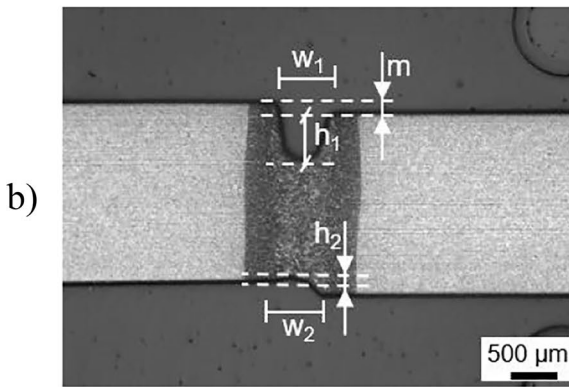
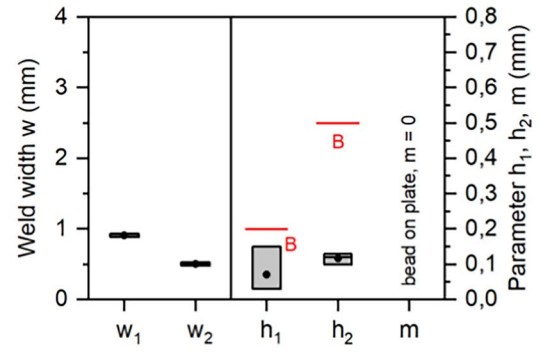
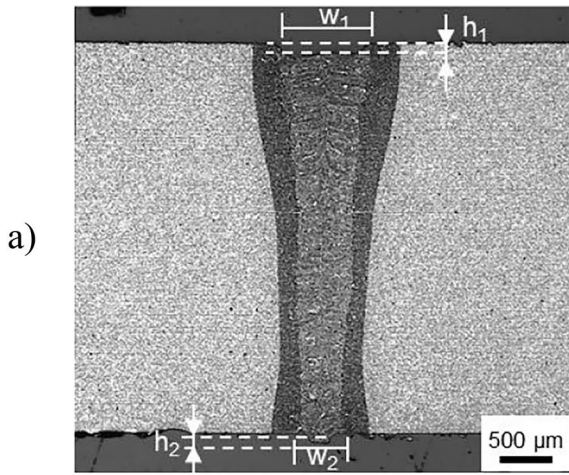




**Fig. 3** Weld seam macrographs and geometric characterization (upper weld bead undercut  $h_1$ , upper weld bead width  $w_1$ , misalignment  $m$ , excess penetration  $h_2$ , root width  $w_2$ ) for specimens welded without gap (a) and different gap bridging properties using focussed laser beam (b), defocussed laser beam (c), and laser beam oscillation (d)

specimen types. Differing from the standard procedure for the critical distance approach, the maximum results on path A1–A2 were used — which do in most cases coincide with the critical distance evaluation on B1–B2. In some cases, the maximum on path A1–A2 diverges slightly from the maximum on B1–B2, compare Fig. 8: with gap, focused beam. Here, path A1–A2 crosses the local minimum at the top of the graph at approximately 2.86 MPa so the chosen approach yields a slightly bigger stress with 3.04 MPa.

Because a unit-stress was applied, the numerical values of stresses translated directly to factors  $k_{eff}$  for the effective stresses. Remarkably, the critical distance approach yielded consistently larger factors  $k_{eff}$  than the stress averaging approach. Exemplary  $k_{eff}$ -values and their determination are shown in Fig. 8.

$$k_{eff} = \frac{\sigma_{eff}}{\sigma_n} \text{ with } \sigma_n = 1 \text{ MPa}$$

For most of the specimens, the maximum principal stress was determined at the top side, as displayed in Fig. 8. Only two specimens showed the maximum at the bottom side. Over all specimens, a clear trend was visible: The specimens without gap had the lowest stress concentration, specimens welded with gap and focused beam had the highest ones. Gap bridging by beam oscillation and defocusing fell in between. This is illustrated in Fig. 9.

As mentioned above, the parameters  $\rho^*$  and  $a$  theoretically depend on the material strength. In order to empirically identify the values leading to a minimum scatter in the fatigue evaluation,  $\rho^*$  and  $a$  were varied between 0mm and 0.4mm in steps of 0.01mm. The evaluation shows a clear result, Fig. 10. For the stress averaging approach, a minimum scatter of 1 :  $T_S = 1.53$  was achieved for  $\rho^* = 0.33\text{mm}$ . A scatter of 1 :  $T_S = 1.58$  was determined for  $a = 0.08\text{mm}$  in the critical distance approach. These values are quite close to the values recommended for a fatigue assessment  $\rho^* = 0.4\text{mm}$

and  $a = 0.1\text{mm}$ . Therefore, the use of recommended values has been continued in all further evaluations.

## 4 Fatigue strength investigations

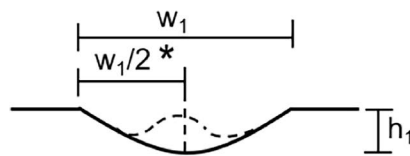
### 4.1 Fatigue test results

The nominal fatigue test results as well as S–N curves based on nominal stress evaluations are presented in Fig. 11. The resulting S–N curves for 50% probability of survival were determined with a fixed slope of  $k=5$ , as recommended for thin sheets [29, 50]. Specimens welded without gap as well as welded with gap and defocused respectively oscillated beam showed comparable fatigue strength results of approximately  $\Delta\sigma \approx 250$  MPa at  $N=1,000,000$  load cycles until specimen fracture. The specimens welded with gap and focused beam showed significantly lower fatigue strength of  $\Delta\sigma \approx 120$  MPa at  $N=500,000$  at large scatters. This was most likely resulting from the weld geometry and present undercuts of large magnitude. For evaluation of weld geometry effects, local fatigue strength approaches were applied. It should be noted that the data shown here was not corrected with regard to resulting load bearing cross sections, e.g., weld undercuts were not considered when calculating the nominal stress. However, the stress magnification due to smaller load carrying weld cross sections of individual test series and specimens did not represent the fatigue strength reduction appropriately.

### 4.2 Fatigue strength evaluation by local approaches

Effective stresses have been derived based on the determined effective stresses and the endurable nominal stresses. The results achieved via both local approaches (critical distance approach and stress averaging approach) were compared to a class FAT 160. This FAT-Class was derived for high tensile residual stress and an effective stress ratio of  $R=0.5$ . Residual stress measurements of the

**Fig. 4** Shape of the undercut and parameters utilized for the ratio  $h_1/w_1$  calculation for specimens welded with gap



\* For the specimens from beam oscillation, it was considered half weld width, because of the undercut geometry (dashed line).

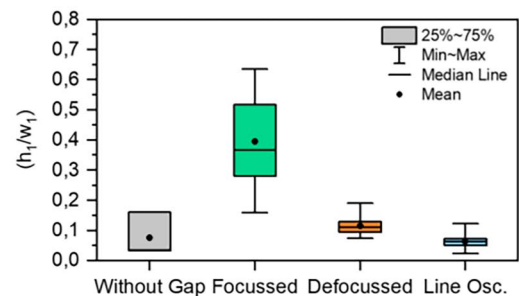


**Fig. 5** Surface residual stress of laser welded 16MnCr5 butt joints with gap longitudinal to the weld (a) and transverse to the weld (b). Transverse direction corresponds to fatigue loading direction. WM: Weld metal; HAZ: Heat affected zone; BM: Base metal

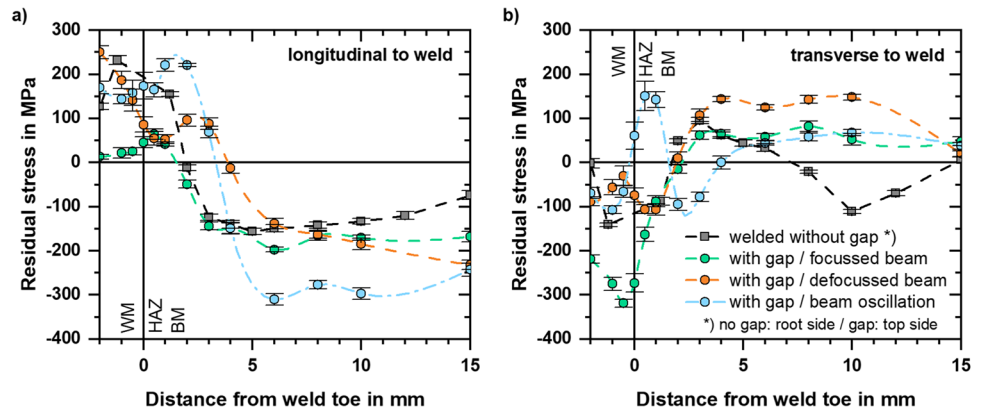
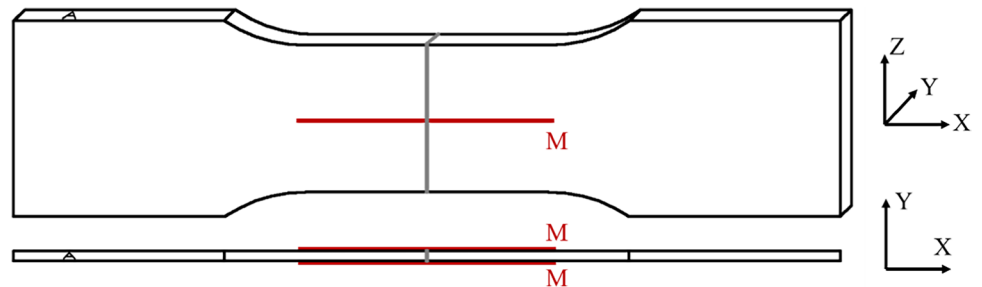


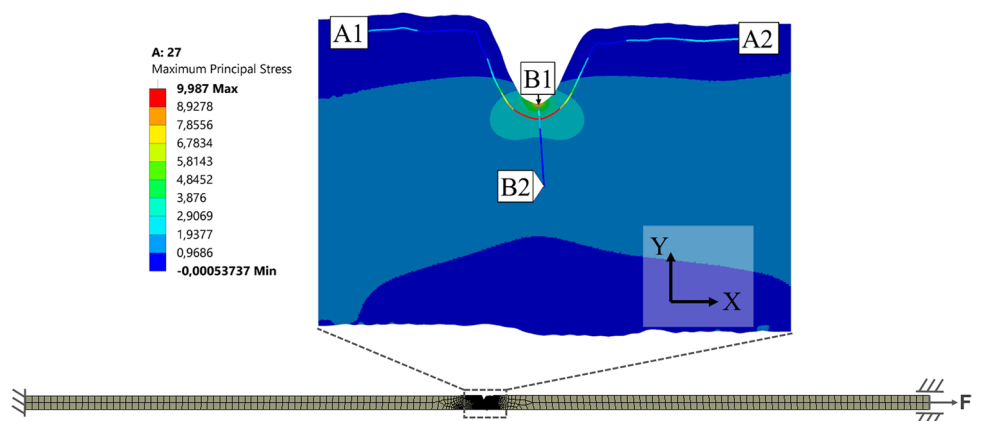
**Fig. 6** Position of the weld profile measurements



welded specimen showed low residual stress, so a fatigue enhancement factor  $f(R)$  should be considered to improve the assessment. According to Hobbacher [24] a so-called bonus factor  $f(R)$  can be calculated for low residual stresses to  $f(R) = -0.4 \cdot R + 1.2$ . For specimens welded with gap  $f(R=0.1) = 1.16$  and for specimen welded without gap  $f(R=0) = 1.2$  was applicable. By scaling the experimental data with these factors and  $k_{eff}$ , all specimen types can be evaluated with FAT 160. The assessed  $\Delta\sigma$  is calculated according to the following formula:

$$\Delta\sigma_{eff} = \frac{\Delta\sigma_n}{f(R)} \cdot k_{eff}$$

**Fig. 7** Finite-Element analyses of a specimen welded with gap and focussed beam — Maximum principal stress in weld proximity; result paths used for critical distance (A1–A2) and stress averaging approach (B1–B2); color on paths not to scale



Assessed S–N curves are presented in Figs. 12 and 13. The same data points as in Fig. 11 were used, but all stress ranges were individually scaled on the Y-axis according to the formula above. As expected, the numerical values of all stresses increased, moving all data points upwards. Additionally, the specimens welded with gap and with focused beam were no longer an outlier of the data sets, as shown in Fig. 11. Both approaches yielded conservative results when evaluated with the FAT 160 design line. The evaluation according to the critical distance approach was slightly more conservative compared to the evaluation according to the stress averaging approach, in which one of the 42 test results examined lied in the non-conservative range.

**Fig. 8** Exemplary path results used for critical distance (a) and stress averaging (b) approaches. Only a selection of specimens is displayed

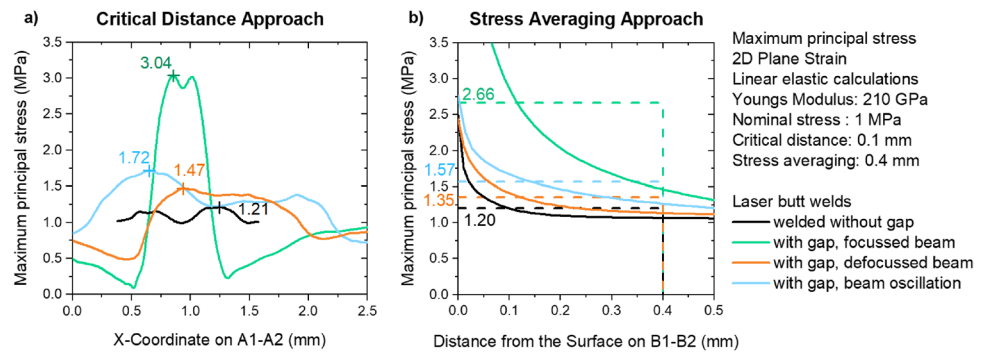


**Fig. 9** Box-plots of  $k_{eff}$  of modeled specimens, grouped by welding parameters. Evaluation approaches critical distance (a) left and stress averaging (b) right

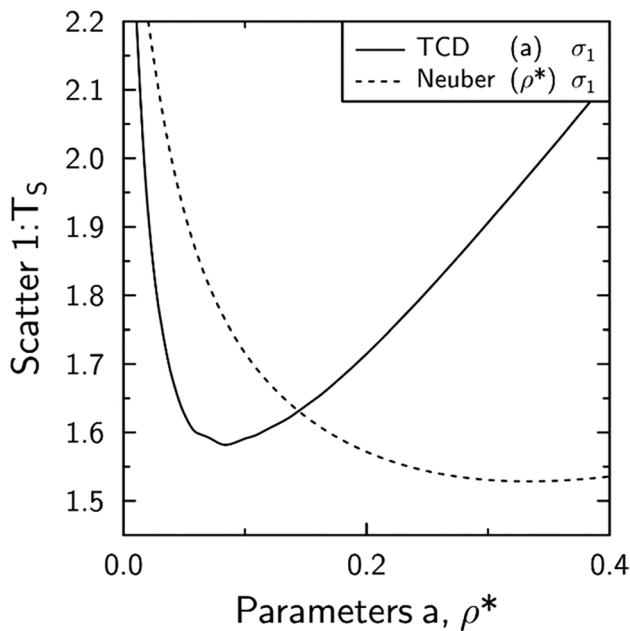
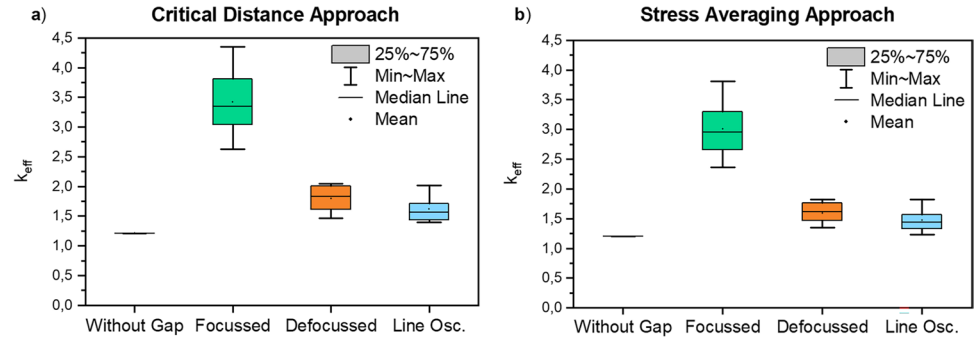


**Fig. 10** Empirical evaluation for the parameters  $\rho^*$  and  $a$  leading to the lowest scatter in the fatigue evaluation

In a statistical evaluation, an S–N curve was derived for each approach. The determined scatter is a value for the assessment reliability. In comparison to the nominal stress approach, the severe differences between weld parameter sets were eliminated by the assessment with local approaches. Thus, a single scatter over all weld groups

became applicable and  $1:T_S$  was identified to 1.53 (stress averaging approach) and 1.61 (critical distance approach). This, combined with largely conservative results, shows that both local approaches can be used to evaluate laser welds with and without gap successfully. The large scatter of the specimens within their weldment groups was also reduced by this evaluation.

## 5 Discussion and conclusions

Gap bridging in laser welding was successfully conducted at reduced ambient pressure by welding with focused, defocused beam and by beam oscillation. The weld quality, especially the weld width and the undercut depth were highly dependent on the welding strategy applied. The weld quality according to ISO 13919-1 was evaluated and a clear correlation of weld strategy and weld quality parameters was proven. It was found that large scatter of local weld geometry parameters resulted in large scatter of fatigue data consequently. Such large scatter needs to be addressed in design of such welded components accordingly. Additionally, the ratio of  $(h_f/w_f)$  was determined and found to correlate with weld strategies applied. Defocussed beam and beam oscillation resulted in comparable weld quality parameters, while the focussed beam showed significantly worse quality parameters. The scatter of the derived S–N curves in Figs. 12 and 13 is mainly caused by the large scatter of each test series welded with gap. Even though a separate FE-model was set

**Fig. 11** Fatigue test data and nominal stress S-N curves of laser welded 16MnCr5 butt joints welded without and with gap. No correction for different R-ratios was applied

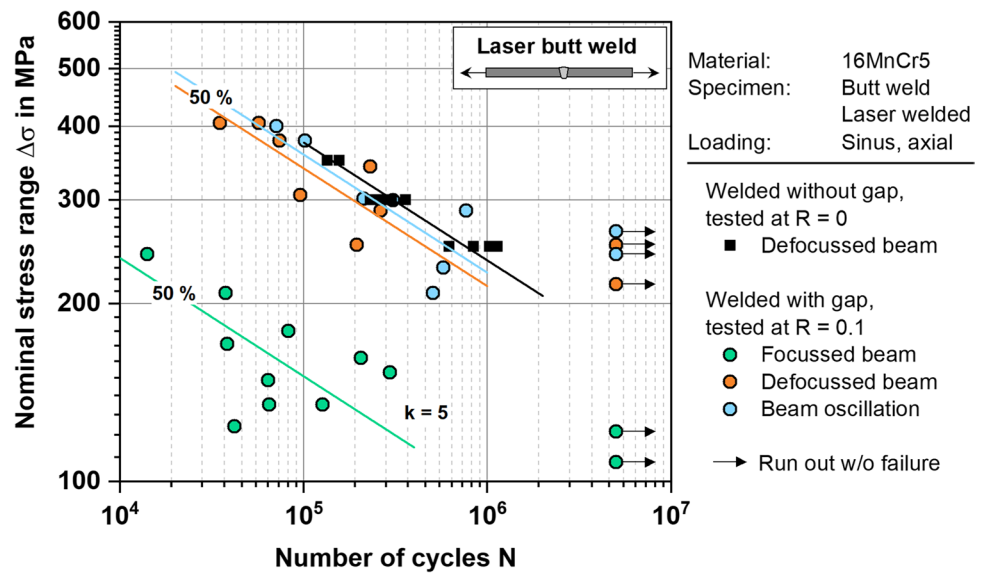
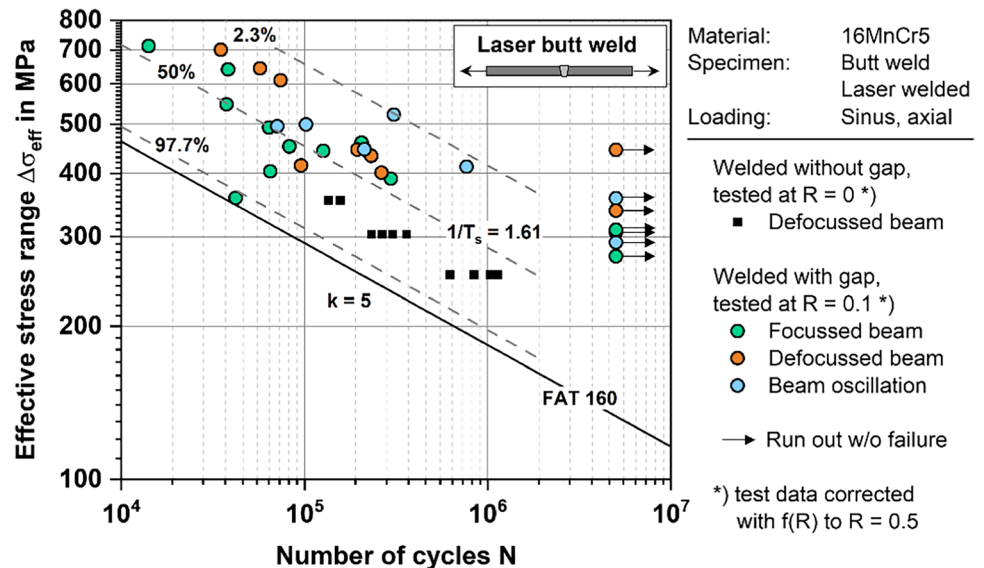


**Fig. 12** Fatigue test results evaluated by the critical distance approach with  $a=0.1$  mm and corrected for  $R=0.5$



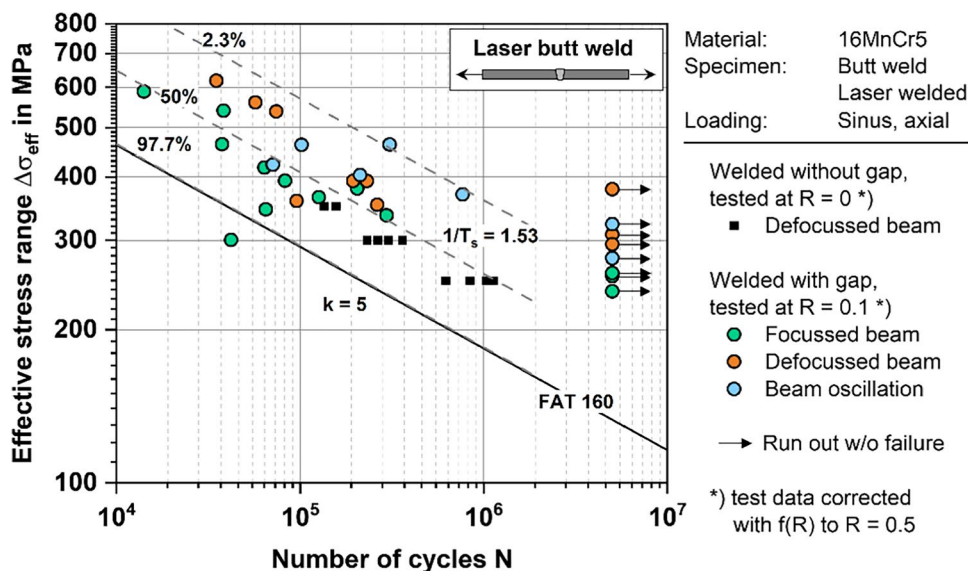
up for each specimen, the scatter is still quite large. Two assumptions may explain the scatter: Firstly, the fatigue critical cross section may not have been modeled, either because it was not included in the line scans or because the manual selection process did not identify the worst case scan appropriately. Secondly, a 2D-model may not be able to describe the real stress state. For future research the modeling of the fatigue critical cross section may be ensured by using a full 3D-surface scan of specimens.

The determined weld quality parameters were found to correlate with fatigue test results. The data from specimens welded with gap and focussed beam had shown significantly lower fatigue strength and large scatter compared to other test series. These other series showed comparable quality

parameters and similar fatigue strength, regardless whether the samples were welded with gap or without gap. Accordingly, effects of defect could be described in good approximation by weld quality parameters applied.

The scatter of fatigue data was significantly reduced by the application of local fatigue evaluation concepts. The standard values of  $\rho^*$  and  $a$  resulted in scatter close to the minimum scatter identified in the identification process, Fig. 10. The high hardness did not seem to have an effect on these parameters. Both applied concepts, stress averaging and critical distance approach, were able to merge the split fatigue test data of the nominal stress approach into a single set. This data could be compared to design S-N curve FAT 160 and  $k=5$ , which was well fitting and conservative

**Fig. 13** Fatigue test results evaluated by the stress averaging approach with  $\rho^* = 0.4$  mm and corrected for  $R = 0.5$



for both approaches. Thus, it has been shown that the butt welds made from 16MnCr5 could be evaluated conservatively if local stress raising effects were considered in the calculation model.

## 6 Summary

Butt welds made from 16MnCr5 were laser welded with and without gap while different gap bridging strategies were applied. The weld quality of all test series was examined based on weld profile measurements and micrographs. Fatigue testing was conducted and correlation of weld quality and fatigue test results was observed. All data was assessed by means of local fatigue strength approaches, i.e., the critical distance approach and the stress averaging approach.

It was found that the fatigue strength of welds of varying quality could be evaluated by FAT 160 if these local approaches were applied and local weld geometry parameters were accounted for.

**Funding** Open Access funding enabled and organized by Projekt DEAL. *Work conducted at TU Braunschweig:* The IGF-research project 19.732 N of the Research Association FOSTA Forschungsvereinigung Stahlanwendung e.V. was funded by the AiF within the program to promote Joint Industrial Research (IGF) by the Federal Ministry for Economic Affairs and Energy, following a decision by the German Bundestag.

*Work conducted at TU Darmstadt:* Parts of the results presented here were developed in the IGF project 20.621B. The authors thank the German Federal Ministry for Economic Affairs and Energy (BMWi) and the German Federation of Industrial Research Associations (AiF) as well as the German Association for Welding and allied processes e. V (DVS) for the financial support.

## Declarations

**Conflict of interest** The authors declare no competing interests.

**Open Access** This article is licensed under a Creative Commons Attribution 4.0 International License, which permits use, sharing, adaptation, distribution and reproduction in any medium or format, as long as you give appropriate credit to the original author(s) and the source, provide a link to the Creative Commons licence, and indicate if changes were made. The images or other third party material in this article are included in the article's Creative Commons licence, unless indicated otherwise in a credit line to the material. If material is not included in the article's Creative Commons licence and your intended use is not permitted by statutory regulation or exceeds the permitted use, you will need to obtain permission directly from the copyright holder. To view a copy of this licence, visit <http://creativecommons.org/licenses/by/4.0/>.

## References

- Vänskä M, Salminen A (2012) Laser welding of stainless steel self-steering tube-to-tube joints with oscillating mirror. *Proc Inst Mech Eng Part B J Eng Manufact Jg* 226(4):632–640. <https://doi.org/10.1177/0954405411425114>
- Müller A, Goecke S-F, Albert F, Sievi P, Baum S (2013) Nahtgeführtes Laserstrahl-Remoteschweißen mit örtlicher Strahloszillation. *Schweißen und Schneiden, Jg* 65(9):631–635
- Fixemer P, Albert F, Sievi P, Graham T (2015) Seam guided laser remote welding with automated gap bridging. *LTI, Jg* 12(2):38–41. <https://doi.org/10.1002/latj.201500012>
- Hesse A-C, Hensel J, Nitschke-Pagel T, Dilger K (2019) Investigations on the fatigue strength of beam-welded butt joints taking the weld quality into account. *Weld World, Jg* 63(5):1303–1313. <https://doi.org/10.1007/s40194-019-00774-5>
- Y. Arata, N. Abe, T. Oda und N. Tsujii, “Fundamental phenomena during vacuum laser welding” in S. 1–7.
- S. Katayama, Y. Kobayashi, M. Mizutani und A. Matsunawa, “Effect of vacuum on penetration and defects in laser welding” (englisch), *J. Laser Appl., Jg* 13, Nr. 5, S. 187, 2001.

7. Börner C, Krüssel T, Dilger K, Dorsch F (2013) “Process characteristics of laser beam welding at reduced ambient pressure” in SPIE LASE. California, USA, San Francisco, p 86030M
8. Jiang M, Tao W, Chen Y, Li F (2019) Comparison of processing window in full penetration laser welding of thick high-strength steel under atmosphere and sub-atmosphere. *Optics Laser Technol Jg* 109:449–455. <https://doi.org/10.1016/j.optlastec.2018.08.023>
9. S. Katayama, Y. Abe, M. Mizutani und Y. Kawahito, “Deep penetration welding with high power disk lasers in low vacuum” in S. 669–678.
10. U. Reisgen, S. Olschok und S. Jakobs, “Laser beam welding under vacuum of a fine-grained steel” in S. 933–940.
11. Reisgen U, Olschok S, Jakobs S, Turner C (2016) Sound welding of copper: laser beam welding in vacuum. *Phys Proc Jg* 83:447–454. <https://doi.org/10.1016/j.phpro.2016.08.046>
12. Luo Y, Tang X, Deng S, Lu F, Chen Q, Cui H (2016) Dynamic coupling between molten pool and metallic vapor ejection for fiber laser welding under subatmospheric pressure. *J Mater Proc Technol Jg* 229:431–438. <https://doi.org/10.1016/j.jmatprotec.2015.09.048>
13. Brock C, Hohenstein R, Schmidt M (2014) Mechanisms of vapour plume formation in laser deep penetration welding. *Optics Lasers Eng Jg* 58:93–101. <https://doi.org/10.1016/j.optlaseng.2014.02.001>
14. C. Börner, K. Dilger, V. Rominger, T. Harrer, T. Krüssel und T. Löwer, “Influence of ambient pressure on spattering and weld seam quality in laser beam welding with the solid-state laser” in S. 621–629.
15. A. Heider, T. Engelhardt, R. Weber und T. Graf, “Influence of ambient pressure on spatter formation during laser welding of copper” (en), *Proc Lasers Manufact Confer Munich*, 2015.
16. Sun Z, Kuo M (1999) Bridging the joint gap with wire feed laser welding. *J Mater Proc Technol Jg* 87(1–3):213–222. [https://doi.org/10.1016/S0924-0136\(98\)00346-X](https://doi.org/10.1016/S0924-0136(98)00346-X)
17. Aalderink BJ, Pathiraj B, Aarts RGKM (2010) Seam gap bridging of laser based processes for the welding of aluminium sheets for industrial applications. *Int J Adv Manuf Technol Jg* 48(1–4):143–154. <https://doi.org/10.1007/s00170-009-2270-x>
18. Schultz V, Seefeld T, Vollertsen F (2014) Gap bridging ability in laser beam welding of thin aluminum sheets. *Phys Proc Jg* 56:545–553. <https://doi.org/10.1016/j.phpro.2014.08.037>
19. Albert F, Marben P, Graham T (2017) Remote laser welding of steel and aluminum alloys. *LTJ Jg* 14(1):32–35. <https://doi.org/10.1002/latj.201700002>
20. Fixemer P, Albert F, Sievi P, Graham T (2015) “Seam guided laser remote welding with automated gap bridging: increased process windows by online recognition of gap situation” (en). *LTJ Jg* 12(2):38–41. <https://doi.org/10.1002/latj.201500012>
21. M. Köhler, T. Tóth, A. Kreybohm, J. Hensel und K. Dilger, “Effects of reduced ambient pressure and beam oscillation on gap bridging ability during solid-state laser beam welding”, *JMMP*, Jg. 4, Nr. 2, S. 40, 2020, <https://doi.org/10.3390/jmmp4020040>.
22. *ISO 5817:2014-06 - Welding - fusion-welded joints in steel, nickel, titanium and their alloys (beam welding excluded) - quality levels for imperfections (ISO 5817:2014)*, Berlin.
23. *ISO 13919-1:2020-03 - Electron and laser-beam welded joints - requirements and recommendations on quality levels for imperfections - part 1: Steel, nickel, titanium and their alloys (ISO 13919-1:2019)*, Berlin.
24. A. F. Hobbacher, *Recommendations for fatigue design of welded joints and components*. Springer International Publishing, 2016.
25. Hobbacher A, Kassner M (2012) On relation between fatigue properties of welded joints, quality criteria and groups in Iso 5817. *Weld World Jg* 56(11–12):153–169. <https://doi.org/10.1007/BF03321405>
26. Lillemäe I, Remes H, Liinalampi S, Itävuo A (2016) Influence of weld quality on the fatigue strength of thin normal and high strength steel butt joints. *Weld World Jg* 60(4):731–740. <https://doi.org/10.1007/s40194-016-0326-8>
27. Stenberg T, Barsoum Z, Åstrand E, Öberg AE, Schneider C, Hedegård J (2017) Quality control and assurance in fabrication of welded structures subjected to fatigue loading. *Weld World Jg* 61(5):1003–1015. <https://doi.org/10.1007/s40194-017-0490-5>
28. M. Kassner, M. KÜppers, C. M. Sonsino, G. Bieker und C. Moser, “Fatigue design of welded components of railway vehicles — influence of manufacturing conditions and weld quality”, *Weld World*, Jg. 54, 9–10, R267–R278, 2010, <https://doi.org/10.1007/BF03266739>.
29. Fricke W et al (2015) Fatigue strength of laser-welded thin-plate ship structures based on nominal and structural hot-spot stress approach. *Ships Offshore Struct Jg* 10(1):39–44. <https://doi.org/10.1080/17445302.2013.850208>
30. Liinalampi S, Remes H, Romanoff J (2019) Influence of three-dimensional weld undercut geometry on fatigue-effective stress. *Weld World Jg* 63(2):277–291. <https://doi.org/10.1007/s40194-018-0658-7>
31. Radaj D (2006) Cetin Morris Sonsino und Wolfgang Fricke. Woodhead Publishing Limited, Fatigue assessment of welded joints by local approaches
32. Zhang G, Richter B (2000) A new approach to the numerical fatigue-life prediction of spot-welded structures. *Fat Frac Eng Mat Struct Jg* 23(6):499–508. <https://doi.org/10.1046/j.1460-2695.2000.00316.x>
33. Cetin Morris Sonsino, W. Fricke, F. de Bruyne, A. Hoppe, A. Ahmadi und G. Zhang, “Notch stress concepts for the fatigue assessment of welded joints – background and applications”, *Int J Fatigue*, Jg. 34, Nr. 1, S. 2–16, 2012, <https://doi.org/10.1016/j.ijfatigue.2010.04.011>.
34. Cetin Morris Sonsino (2009) A consideration of allowable equivalent stresses for fatigue design of welded joints according to the notch stress concept with reference radii rref = 1.00 and 0.05 mm. *Welding World Jg* 53:64–75. <https://doi.org/10.1007/BF03266705>
35. Baumgartner J (2017) Review and considerations on the fatigue assessment of welded joints using reference radii. *Int J Fatigue Jg* 101:459–468. <https://doi.org/10.1016/j.ijfatigue.2017.01.013>
36. Bruder T, Störzel K, Baumgartner J, Hanselka H (2012) Evaluation of nominal and local stress based approaches for the fatigue assessment of seam welds. *Int J Fatigue Jg* 34(1):86–102. <https://doi.org/10.1016/j.ijfatigue.2011.06.002>
37. J. Baumgartner, A. F. Hobbacher und R. Rennert, “Fatigue assessment of welded thin sheets with the notch stress approach (textendash proposal for recommendations”, *Int J Fatigue Jg*. 140, S. 105844, 2020, <https://doi.org/10.1016/j.ijfatigue.2020.105844>.
38. Baumgartner J (2019) Halid Can Yıldırım und Zuheir Barsoum, “Fatigue strength assessment of TIG-dressed welded steel joints by local approaches.” *Int J Fatigue Jg* 126(9):72–78. <https://doi.org/10.1016/j.ijfatigue.2019.04.038>
39. Radaj D (ed) (1990) Design and analysis of fatigue resistant welded structures. Woodhead Publishing, Cambridge
40. Neuber H (1958) Kerbspannungslehre, 2. Springer Verlag, Aufl
41. Neuber H (1968) Über die Berücksichtigung der Spannungskonzentration bei Festigkeitsberechnungen. *Konstruktion*, Jg 20(7):245–251
42. H. F. Moore, “A study of size effect and notch sensitivity in fatigue tests of steel” in *Proc. ASTM*, 1945, S. 507–531.
43. R.E. Peterson, *Metal fatigue*. McGraw-Hill Book Company, Inc, 1959.
44. Taylor D (1999) Geometrical effects in fatigue: a unifying theoretical model. *Int J Fatigue Jg* 21(5):413–420. [https://doi.org/10.1016/S0142-1123\(99\)00007-9](https://doi.org/10.1016/S0142-1123(99)00007-9)

45. Siebel E, Stieler M (1955) Ungleichförmige Spannungsverteilung bei schwingender Beanspruchung. VDI Zeitschrift Jg 97:121–126
46. Ronald Rennert, Eckehard Kullig, Michael Vormwald, Alfons Esderts und Dieter Siegele, *FKM guideline - analytical strength assessment of components* (english).
47. Baumgartner J, Lipp K, Bruder T, Kaufmann H (2011) Design methods for reliable fatigue assessment of PM components. *Materialwissenschaft und Werkstofftechnik*, Jg 42(10):894–903. <https://doi.org/10.1002/mawe.201100869>
48. Baumgartner J, Schmidt H, Ince E, Melz T, Dilger K (2015) “Fatigue assessment of welded joints using stress averaging and critical distance approaches” (English). *Welding World Jg* 59(5):731–742. <https://doi.org/10.1007/s40194-015-0248-x>
49. Remes H, Fricke W (2014) Influencing factors on fatigue strength of welded thin plates based on structural stress assessment. *Weld World Jg* 58(6):915–923. <https://doi.org/10.1007/s40194-014-0170-7>
50. Sonsino CM, Bruder T, Baumgartner J (2010) S-N Lines for welded thin joints — suggested slopes and FAT values for applying the notch stress concept with various reference radii. *Weld World Jg* 54(11–12):R375–R392. <https://doi.org/10.1007/BF03266752>

**Publisher's note** Springer Nature remains neutral with regard to jurisdictional claims in published maps and institutional affiliations.